Research Square

Preprints are preliminary reports that have not undergone peer review.
They should not be considered conclusive, used to inform clinical practice,
or referenced by the media as validated information.

On the Relativistic Harmonic Oscillator

Yair Zarmi (zarmi@bgu.ac.il)
Ben-Gurion University of the Negev - Sede Boqer Campus https://orcid.org/0000-0001-8830-9667

Research Article

Keywords: Relativistic harmonic oscillator, weak-relativistic limit, extreme-relativistic limit, boundary-layer phenomenon

Posted Date: January 4th, 2022

DOI: https://doi.org/10.21203/rs.3.rs-1156316/v1

License: This work is licensed under a Creative Commons Attribution 4.0 International License.
Read Full License

On the Relativistic Harmonic Oscillator

Yair Zarmi
Jacob Blaustein Institutes for Desert Research
Ben-Gurion University of the Negev
Midreshet Ben-Gurion, 8499000, Israel

Abstract
In view of interest in relativistic harmonic oscillations in media, through which the speed of light is orders of magnitude smaller than in vacuum, the solution of the equation of motion is analyzed in the extreme- and weak-relativistic limits. Using scaled variables, it is shown rigorously how the equation of motion exhibits the characteristics of a boundary-layer problem in the extreme-relativistic limit: The solution differs from a sharp asymptotic pattern only around the turning points of oscillations over a vanishingly small fraction of the period. The sharp asymptotic pattern of the solution is a saw-tooth composed of linear segments. The velocity profile tends to a periodic step function and the phase-space plot tends to a rectangle. An expansion of the solution in terms of a small parameter that measures the proximity to the limit $(v/c) \to 1$ yields an excellent approximation for the solution throughout the whole period of oscillations. In the weak-relativistic limit the same approach yields an approximation to the solution that is significantly better than in traditional asymptotic expansion procedures.

Keywords: Relativistic harmonic oscillator; weak-relativistic limit, extreme-relativistic limit; boundary-layer phenomenon.

Email: zarmi@bgu.ac.il

Orcid: 0000-0001-8830-9667

1. Introduction

Over the years, the study of relativistic oscillations has progressed in several avenues including the study of the Dirac oscillator theoretically [1-4] and experimentally [5], and the quantization of the relativistic harmonic oscillator [6-11]. Oscillations in the weak-relativistic limit have been of interest in Plasma Physics [12-24]. Results have been attained by either generating numerical solutions, or by expansions in powers of β^2 ($\beta = (\mathrm{Max}|\dot{x}|)/c$) in the weak-relativistic limit [25-35]. Owing to the limitation of the validity in time of approximate solutions obtained by asymptotic expansion methods, typically, the lowest-order approximation (($O(\beta^2)$) in such analyses has a 1-2% error relative to the numerical solution only up to $\beta \approx 0.2$.

The absence of tools for analyzing the oscillatory motion of a mass governed by the equation of motion of the RHO in the extreme-relativistic limit has, most probably, been a consequence of the fact that, in this limit, the acceleration close to the turning point of the oscillations grows indefinitely. Unless the oscillator is placed in outer space far from any massive object, at such high acceleration, Special Relativity fails and General Relativistic effects emerge.

Interest in the RHO, in both weak- and extreme-relativistic limits has won renewed attention in the study of media, through which light propagates at velocities that are much lower than its speed in vacuum, so that General Relativity is of no concern. A recent example is that of the dynamics of an oscillator composed of ultra-cold Bose-condensed lithium atoms in the third band of an optical lattice [36, 37]. The energy-momentum relation of the atoms is nearly identical to that of a massive relativistic particle, with an effective mass. The effective speed of light, c, is very low (143 mm/s).

In this paper, the RHO is analyzed in the weak- and extreme- relativistic limits. Preliminary information is presented in Section 2. Exploiting the known closed-form expressions of the period, T, and the oscillation amplitude, $x_{\max}$, the time and position variables, t and x, are transformed into dimensionless variables, θ and η, respectively. η is (2π)-periodic in θ and bounded: $|\eta| \leq 1$. This transformation, presented in Section 3, relieves the analysis in the weak-relativistic limit of the re-

striction on the validity in time of approximate solutions, encountered in standard asymptotic expansion perturbative analyses. In addition, it naturally leads to a novel approach to the analysis of the extreme-relativistic limit.

The weak-relativistic limit is discussed in Section 4 through a Normal Form expansion [38-45]. As the solution is (2 π)-periodic in θ, there is no need to worry about the growth of secular errors in the approximate solution for $\theta \gg 1$. A direct consequence is that the error in the approximate solution turns out to remain very small up to rather high values of β. For example, in an expansion through $O(\beta^2)$, the approximations for the dimensionless position, η, and for the velocity, η', agree with the full numerical solution within a fraction of 1% up to $\beta \approx 0.6$ and $\beta \approx 0.45$, respectively.

The expansion in powers of β^2 fails in the extreme relativistic limit ($\beta \to 1$): The error in the approximation for the velocity, η', reaches $O(1)$. In this limit, over most of the period of oscillations, $\dot{x}$ oscillates between two constant values, $\pm v_{max}$, ($v_{max} = c \cdot \beta$) and is reduced to zero rapidly over a short time interval near the turning point. This suggests that the RHO becomes a boundary-layer problem. The analysis presented in Section 5 confirms this conjecture. Introducing a small parameter, μ, defined by $\beta^2 = 1 - \mu^4$ ($\mu \ll 1$ for $\beta \to 1$), the coefficient multiplying the term with the highest derivative in the equation of motion for η is $O(\mu^2)$ - a characteristic of boundary-layer problems.

Near the turning point ($\theta = 0$), the velocity varies rapidly over a range of $O(\mu^2)$ in θ. Hence, for finding an approximate solution for η over this narrow range in the extreme-relativistic limit, a variable transformation is required, $\theta = \mu^2 z$, so that z is of $O(1)$. The resulting expansion of the solution in powers of μ^2, expected to provide a good approximation to the solution near the turning point ($\theta = O(\mu^2)$ ($z = O(1)$)), generates an excellent approximation to the solution for $0 \leq \theta \leq 2\pi$, even in the lowest order in μ^2, for small μ. Unique features of the Fourier expansion of the solution are discussed in Section 6.

2. Preliminaries

The dynamical equation of the RHO is:

$$m\omega_0^{\,2}x + m\frac{\ddot{x}}{\left(1-\left(x'/c\right)\right)^{3/2}} = 0 \quad . \tag{1}$$

The total energy is given by:

$$E = \frac{1}{2}m\omega_0^{\,2}x^2 + \frac{mc^2}{\sqrt{1-\left(\dot{x}/c\right)^2}} = \frac{mc^2}{\sqrt{1-\beta^2}} \quad , \quad \left(\beta = \max\left(\left|\dot{x}\right|/c\right)\right). \tag{2}$$

Solving Eq. (2) for $\dot{x}$ yields the period of oscillations [46]:

$$T = \frac{1}{\omega_0}4\sqrt{2}\left(\sqrt{1+\frac{1}{\sqrt{1-\beta^2}}}\,E\left(k\right) - \left(1\Big/\sqrt{1+\frac{1}{\sqrt{1-\beta^2}}}\right)K\left(k\right)\right) \quad , \quad k^2 = \left(\frac{1-\sqrt{1-\beta^2}}{1+\sqrt{1-\beta^2}}\right). \tag{3}$$

In Eq. (3), $E(k)$ and $K(k)$ are the complete elliptic integrals [47]:

$$E\left(k\right) = \int_0^{\pi/2}\sqrt{1-k^2\sin\varphi^2}\,d\varphi \quad , \quad K\left(k\right) = \int_0^{\pi/2}\left(1\Big/\sqrt{1-k^2\sin\varphi^2}\right)d\varphi \; . \tag{4}$$

The maximal values of the amplitude of oscillations and of the velocity are obtained by setting $\dot{x}=0$ and $x = 0$, respectively, in Eq. (2), yielding:

$$x_{\max} = \sqrt{2}\frac{c}{\omega_0}\frac{\sqrt{1-\sqrt{1-\beta^2}}}{\left(1-\beta^2\right)^{1/4}} \quad , \quad \dot{x}_{\max} = \beta c \quad . \tag{5}$$

In the limit of small relativistic effects ($\beta \ll 1$), the expansion of E, T (using expansions of elliptic functions presented in [47]) and $x_{\max}$ in powers of β^2 is given by:

$$\begin{aligned}
E &= mc^2\left(1+\frac{1}{2}\beta^2+\frac{3}{8}\beta^4+\frac{5}{16}\beta^6+O\left(\beta^8\right)\right)\\
T &= \frac{2\pi}{\omega_0}\left(1+\frac{3}{16}\beta^2+\frac{129}{1024}\beta^4+\frac{1595}{16384}\beta^6+O\left(\beta^8\right)\right)\\
x_{\max} &= \frac{\beta c}{\omega_0}\left(1+\frac{3}{8}\beta^2+\frac{31}{128}\beta^4+\frac{187}{1024}\beta^6+O\left(\beta^8\right)\right)\\
\frac{x_{\max}}{T} &= \frac{\beta c}{2\pi}\left(1+\frac{3}{16}\beta^2+\frac{83}{1024}\beta^4+\frac{761}{16384}\beta^6+O\left(\beta^8\right)\right)
\end{aligned} \tag{6}$$

In the far relativistic limit ($\beta \approx 1$) it turns out to be convenient to define a new small parameter:

$$\beta^2 = 1 - \mu^4 \quad , \quad (\mu \ll 1) . \tag{7}$$

Eq. (6) is then replaced by (the expansion of the elliptic integrals can be found in Ref. [47]):

$$\begin{aligned} E &= \frac{mc^2}{\mu^2} \\ T &= \frac{4\sqrt{2}}{\omega_0}\frac{1}{\mu}\left(1 - \mu^4\frac{3 - 6\log 2 + 4\log\mu}{16} + O\left(\mu^8\right)\right) \\ x_{\max} &= \sqrt{2}\frac{c}{\omega_0}\frac{1}{\mu}\left(1 - \frac{1}{2}\mu^2 - \frac{1}{8}\mu^4 - \frac{1}{16}\mu^6 + O\left(\mu^8\right)\right) \\ \frac{x_{\max}}{T} &= \frac{c}{4}\left(1 - \frac{1}{2}\mu^2 + \frac{1}{16}\mu^4\left(1 - 6\log 2 + 4\log\mu\right) - \frac{1}{32}\mu^6\left(5 - 6\log 2 + 4\log\mu\right) + O\left(\mu^8\right)\right) \end{aligned} \quad . \tag{8}$$

Note that both T and $x_{\max}$ tend to infinity as $E^{1/2}$.

Fig. 1 shows the phase-space plot of the numerical solution of Eq. (1) for a sequence of values of β. x and t are expressed in terms of dimensionless entities:

$$\tau = \omega_0 t \quad , \quad X(\tau) = (\omega_0/c)\,x(\tau/\omega_0) . \tag{9}$$

The emergence of boundary-layer characteristics at high values of β is visible: $X'(\tau)$ changes from a constant value to zero over a small range in time near the turning point.

3. Scaled equation

Rescaling x and t as follows:

$$x(t) = x_{\max}\,\eta(\theta) \quad , \quad t = (T/2\pi\omega_0)\theta , \tag{10}$$

Eq. (1) becomes

$$\eta(\theta) + \left(\frac{2\pi}{\omega_0 T}\right)^2 \frac{\eta''(\theta)}{\left(1 - \left(\frac{2\pi x_{\max}}{cT}\right)^2 \eta'(\theta)^2\right)^{3/2}} = 0 . \tag{11}$$

$\eta(\theta)$ is (2π)-periodic in θ and bounded: $|\eta(\theta)| \le 1$. Exploiting Eqs. (10) and (6), yields that the maximal values of η and η' are both finite for all $0 \le \beta^2 \le 1$:

$$\eta_{\max} \equiv \max\left(\left|\eta\right|\right) = 1$$

$$\eta'_{\max} \equiv \max\left|\left(\eta'\left(\theta\right)\right)\right| = \left(\frac{\beta c T}{2\pi x_{\max}}\right) \rightarrow \begin{cases} 1 - \frac{3}{16}\beta^2 + O\left(\beta^4\right) & \beta \rightarrow 0 \\ \frac{2}{\pi} + \frac{\mu^2}{\pi} + O\left(\mu^4 \log \mu\right) & \beta \rightarrow 1 \end{cases} . \qquad (12)$$

Figs. 2, 3 and 4 show the dependence of the solution on β. For $\beta \ll 1$, the phase-space plot is very close to a circle. As β is increased, it approaches a rectangle. Concurrently, η' evolves from a sine-like function of θ to a periodic step function and that of η – to a sequence of almost straight lines.

For $\beta \ll 1$, Eq. (11) is reduced to the equation of a classical harmonic oscillator perturbed by a small nonlinear term:

$$\eta\left(\theta\right) + \left(1 + O\left(\beta^2\right)\right)\frac{\eta''\left(\theta\right)}{\left(1 - \beta^2\left(1 + O\left(\beta^2\right)\right)\eta'\left(\theta\right)^2\right)^{3/2}} = 0 . \qquad (13)$$

Hence, this calls for an expansion in powers of β^2.

In the extreme-relativistic limit, Eq. (11) becomes a boundary-value problem. Using Eqs. (7) and (8), the highest derivative is multiplied by a small coefficient:

$$\eta\left(\theta\right) + \frac{\pi^2}{8}\mu^2\left(1 + O\left(\mu^4 \log \mu\right)\right)\frac{\eta''\left(\theta\right)}{\left(1 - \left(\frac{\pi^2}{4}\right)\left(1 - \mu^2 + O\left(\mu^4\right)\right)\eta'\left(\theta\right)^2\right)^{3/2}} = 0 . \qquad (14)$$

4. Weak-relativistic limit

A convenient way to analyze Eq. (11) is to transform it to a first-order equation for a complex entity:

$$z\left(\theta\right) = \eta\left(\theta\right) + i\eta'\left(\theta\right) . \qquad (15)$$

Expressing η and η' in terms of z and z^*, Eq. (11) is transformed into:

$$z'\left(\theta\right) = \frac{\left(z\left(\theta\right) - z^*\left(\theta\right)\right)}{2i} + i\left\{-\left(\frac{\omega_0 T}{2\pi}\right)^2 \frac{\left(z\left(\theta\right) + z^*\left(\theta\right)\right)}{2}\left(1 - \left(\frac{2\pi x_{\max}}{cT}\right)^2\left(\frac{\left(z\left(\theta\right) - z^*\left(\theta\right)\right)}{2i}\right)^2\right)^{3/2}\right\} . \qquad (16)$$

The boundary conditions at the turning point are:

$$\eta(0)=\frac{z(0)+z^*(0)}{2}=1 \quad , \quad \eta'(0)=\frac{z(0)-z^*(0)}{2i}=0 \, . \tag{17}$$

One now writes $z(\theta)$ as:

$$z(\theta)=z_0(\theta)+\beta^2 z_2(\theta)+\beta^4 z_4(\theta)+\beta^6 z_6(\theta)+\ldots \tag{18}$$

and exploits the expansion of T and $x_{\max}$ (Eq. (6)) to obtain an expansion of Eq. (16) in powers of β^2.

The zero-order term of this expansion yields:

$$z_0'(\theta)=-i z_0(\theta) \Rightarrow z_0(\theta)=\rho_0 e^{-i(\theta+\theta_0)} \, . \tag{19}$$

Thus, as expected, the zero-order term is (2π)-periodic in θ. The $O(\beta^2)$ term in the expansion of Eq. (16) is:

$$z_2'(\theta)=-i z_2(\theta)-\frac{3}{8} i\left\{\rho_0\left(1-\rho_0{}^2\right)\cos(\theta+\theta_0)+\rho_0{}^3\cos\left(3(\theta+\theta_0)\right)\right\} \, . \tag{20}$$

For the solution to be periodic in θ, the coefficient of the resonant term $\cos(\theta+\theta_0)$ must vanish, yielding

$$\rho_0=1 \, . \tag{21}$$

One now proceeds in the same fashion through higher orders, requiring that the higher-order corrections, z_4 and z_6 of Eq. (18) are periodic in θ (i.e., the coefficients of resonant terms in the dynamical equations for z_4 and z_6 vanish) and that the initial conditions are obeyed by the zero-order term:

$$\frac{z_0(0)+z_0{}^*(0)}{2}=1 \quad , \quad \frac{z_0(0)-z_0{}^*(0)}{2i}=0 \, . \tag{22}$$

The result is the following expression for η:

$$\begin{aligned}\eta(\theta)=\cos\theta+\beta^2\frac{3}{64}(-\cos\theta+\cos3\theta)+\beta^4\left(\frac{-97\cos\theta+72\cos3\theta+25\cos5\theta}{4096}\right)\\ +\beta^6\left(\frac{-11619\cos\theta+6786\cos3\theta+4000\cos5\theta+833\cos7\theta}{786432}\right)+O(\beta^8)\end{aligned} \, . \tag{23}$$

The fact that the period, T, is known explicitly means that the restriction of the validity of the approximation that emerges in well-known asymptotic expansion methods is avoided. (In these methods, the period is approximated by a truncated expansion in powers of the small parameter, limiting the validity of the approximation to times of $O(1)$ or $O(1/\beta^2)$, depending on the analysis method used.) The approximation to the full numerical solution up the rather high values of β is excellent. For $\beta = 0.1$, the maximal relative error generated by the approximate solution of Eq. (23) is, at most, $O(.01\%)$. In expansions through $O(\beta^2)$, $O(\beta^4)$ and $O(\beta^6)$, the approximation for η agrees with the full numerical solution of Eq. (11) within a fraction of 1% up to $\beta \approx 0.6$, 0.7 and 0.8, respectively, for all θ. The approximation for η', agrees with the full numerical solution within a fraction of 1% up to $\beta \approx 0.4$, 0.55 and 0.65, respectively, for all θ. Even for $\beta \approx 0.8$, the relative error of the approximate expression for the amplitude (through $O(\beta^6)$, Eq. (23)) varies between 0 and close to 1% (see Fig. 5) and for the velocity – between 1% and 5% (see Fig. 6).

5. Extreme relativistic limit: A boundary-layer problem

In the extreme relativistic limit, the expansion in powers of β^2 fails. Figs. 7a-c show how the approximate solution (Eq. (23)) begins to deviate from the numerical solution of Eq. (11) as β grows. The errors in η and η' are shown in Figs. 8 and 9, respectively, in a computation through $O(\beta^6)$, for $\beta = 0.99$. The error in η is, at most about 10%. In η', it exceeds 60% near the turning point.

In this limit, the velocity, $\dot{x}$, is constant at ($\pm c\ \beta$) most of the time. It vanishes rapidly over a short time gap near the turning point. (See Fig. 1) In the scaled coordinates, the dependence of η on θ is a straight line, except very close to the turning point (see Fig. 3).

The fact that the system exhibits the characteristics of a boundary layer problem is demonstrated by Eq. (14): The highest derivative in the equation is multiplied by a small parameter. To guide oneself towards a choice of a scaled variable that is appropriate for the analysis of Eq. (11) near the turning point, observe that η' is now very close to zero. Using Eq. (8) for T and x_{max} and replacing η' by

zero in Eq. (14), the $O(\mu^2)$ approximation to the equation becomes:

$$\eta(\theta) + \frac{\pi^2}{8}\mu^2 \eta''(\theta) = 0 \,. \tag{24}$$

For the boundary conditions at the turning point ($\theta = 0$), $\eta(0) = 1$ and $\eta'(0)=0$, Eq. (24) is solved by

$$\eta(\theta) = \cos\left(\frac{2\sqrt{2}}{\pi}\frac{\theta}{\mu}\right) \,. \tag{25}$$

Exploiting the leading-order term in $\eta'_{\max}$ (Eq. (12)), one finds an approximation for θ_S, the value of θ, at which the slope η' from Eq. (25) becomes equal to the constant (maximal) slope that prevails throughout most of the range $0 \le \theta \le (\pi/2)$. Eq. (25) yields:

$$\eta'(\theta_S) \approx -\eta'_{\max} \Rightarrow \theta_S \approx \frac{\pi}{4}\mu^2\left(1 + \frac{1}{2}\mu^2\right). \tag{26}$$

The matching point is of $O(\mu^2)$. For a valid expansion in powers of μ^2 near the turning point, one must, therefore, rescale θ as:

$$\theta = \mu^2 z \,, \tag{27}$$

so that z is of $O(1)$. One now expands $\eta(\theta)$ in powers of μ^2:

$$\eta(\theta) = 1 + \mu^2 F_2(z) + \mu^4 F_4(z) + \mu^6 F_6(z) + O(\mu^8) \quad , \quad \left(z = (\theta/\mu^2)\right). \tag{28}$$

Using Eqs. (28) and (7), one expands Eq. (14) in powers of μ^2, and solves for the higher-order corrections in Eq. (28). The boundary conditions for all F_{2n} are:

$$F_{2n}(z=0) = F_{2n}'(z=0) = 0 \,. \tag{29}$$

Through $O(\mu^6)$, F_{2n} are found to be given by:

$$F_2(z) = \frac{1}{2} - \frac{\sqrt{\pi^2 + 16z^2}}{2\pi} \,, \tag{30}$$

$$F_4(z) = \frac{1}{4} - \frac{\sqrt{\pi^2 + 16z^2}}{4\pi} + \frac{z \arcsin(4z/\pi)}{2\sqrt{\pi^2 + 16z^2}} \,, \tag{31}$$

$$F_6(z)=\frac{1}{4}+\left(-\frac{\pi}{128}-\frac{\pi z}{8\left(\pi^2+16z^2\right)}+\frac{z}{4\sqrt{\pi^2+16z^2}}\right)\arcsin\left(4z/\pi\right)$$
$$-\frac{\pi^3\arcsin\left(4z/\pi\right)^2}{64\left(\pi^2+16z^2\right)^{3/2}}+\frac{\pi}{128}\log\left(\frac{4z+\sqrt{\pi^2+16z^2}}{\pi}\right)$$
$$+\sqrt{\pi^2+16z^2}\left(-\frac{3}{64\pi}-\frac{3\log(2)}{16\pi}+\frac{\log(\mu)}{8\pi}\right)$$
$$+\frac{1}{\sqrt{\pi^2+16z^2}}\left(-\frac{13\pi}{64}+\frac{13\pi}{16}\log(2)-\frac{\pi}{8}\log(\mu)\right) \quad . \qquad (32)$$

Detailed inspection of F_{2n} for 2 n = 2, 4, 6, reveals that they all have the same qualitative dependence on θ. Except very near the turning point ($\theta = 0$) they all tend to a linear dependence on θ. They vanish at roughly the same rate as θ varies from $O(\mu^2)$ down to zero.

The surprising result is that an expansion that was meant to be valid around the turning point ($\theta \approx O(\mu^2)$) yields an excellent approximation for the solution throughout $0 \leq \theta \leq 2\,\pi$ for small μ. For sufficiently small values of μ, an excellent approximation is obtained with just the $O(\mu^2)$ term:

$$\eta(\theta)=1+\mu^2 F_2(z)\,. \qquad (33)$$

Figs. 10 and 11 show a comparison between the approximation, Eq. (33), and the numerical solution of Eq. (11) for $\mu = 0.1$ ($\beta = 0.99995$). θ_S is then ≈ 0.0078. To stress the quality of the approximation, Fig. 12 shows how small the deviation of the approximate solution from the numerical solution remains even for $\theta \gg \theta_S$. Fig. 13 shows the relative error in η'. It remains small for all $0 \leq \theta \leq 2\,\pi$.

Finally, for $\theta = O(1)$, namely, away from the turning point, F4[$z = \theta/\mu^2$] adds a μ^2 contribution. An excellent approximation is obtained by:

$$\eta(\theta)=1+\frac{\mu^2}{2}-\left(\frac{2+\mu^2}{\pi}\right)\theta+O\left(\mu^4\log\mu\right)\,. \qquad (34)$$

6. Fourier expansion

The evolution of the velocity profile, $\eta'(\theta)$, in the extreme relativistic limit ($\beta \to 1$, $\mu \to 0$) into a periodic step function (see Fig. 4) offers unique characteristics for the Fourier spectrum of $\eta'(\theta)$.

The Fourier coefficients tend to the limiting spectrum of the step function, the latter oscillating between $\pm (2/\pi)$ with a cycle length of (2π). The Fourier series for this step function is:

$$\sum_{n=0}^{\infty} a_{2n+1} \sin\left(2n+1\right)\theta \quad , \quad a_{2n+1} = -\frac{8}{\left(2n+1\right)\pi^2} \, . \tag{35}$$

The purpose of this Section is to discuss two aspects. The first is a demonstration of the qualitative difference between the Fourier spectra in the weak- and extremely-relativistic limits. The second is an additional test of the quality of the approximate solution obtained in Section 5.

6.1 Fourier spectra in weekly- and extreme-relativistic limits

Fig. (14) presents a comparison between the β dependence of the Fourier coefficients of $\eta'(\theta)$, obtained from the numerical solution of Eq. (11), and the spectrum of Eq. (35). There is a qualitative difference between the β - dependence of the Fourier coefficients for small β and the μ -dependence for small μ (defined in Eq. (7)). For small β, the spectrum is dominated by a small number of modes. For $\beta \to 0$, the spectrum tends to a single mode, $\sin(\theta)$. The analysis in Section 4 exhibits the β - dependence of the modes for small β: $\sin((2n+1)\theta)$ modes appear in $O(\beta^{2n})$. As β approaches 1, the Fourier coefficients tend to the limiting spectrum, which is $O(1)$ in μ.

6.2 Test of quality of approximate solution in extreme-relativistic limit

In Fig. 15, a comparison between the Fourier coefficients of $\eta'(\theta)$, computed for the approximate solution, Eqs (28) and (32), with those obtained from the numerical solution of Eq. (11) for $\mu = 0.2$ ($\beta = 0.992$) is presented for $1 \le 2n+1 \le 41$. The relative error between the exact numerical and the approximate values is below 5% for $1 \le 2n+1 \le 13$. For $\mu = 0.1$, the error is smaller than 0.5% for all $1 \le 2n+1 \le 41$.

7. Concluding comments

The dynamics of the Relativistic Harmonic Oscillator (RHO) have been analyzed in the weak- and extreme-relativistic limits. Exploiting the fact that the period of oscillations can be computed in closed form and to any desired level of numerical accuracy, and using the scaled variables of Eq.

(10), for $\beta < 1$, a Normal Forms expansion yields a high quality approximation to the solution that is by far better than the standard application of asymptotic expansion methods.

The same formulation allows for the analysis of the extreme-relativistic limit as a boundary-layer problem, leading to a high-quality approximation for the solution for all $0 \leq \theta \leq (2\ \pi)$ for $(1 - \beta)$ « 1.

Statements and Declarations
The author declares that no funds, grants, or other support were received during the preparation of this manuscript.
The author has no relevant financial or non-financial interests to disclose.
1) The author made all contributions to the conception or design of the work. No data acquisition was required. No new software was created.
2) The author drafted the work or revised it critically for important intellectual content;
3) The author approved the version to be published; and
4) The author agrees to be accountable for all aspects of the work in ensuring that questions related to the accuracy or integrity of any part of the work are appropriately investigated and resolved.

Data availability Statement
Data sharing is not applicable to this article, as no datasets were generated or analyzed during the current study.

References

1) A. Bermudez, A. Martin-Delgado and E. Solano, Phys. Rev. E., **A 76**, 041801(R) (2007).
2) S. Longhi, Opt. Lett., **35**, 1302-1304 (2010).
3) S. Longhi, Appl. Phys., **B 104**, 453-468 (2011).
4) R. Gerritsma et al., Phy. Rev. Lett. **106**, 060503 (2011).
5) J.A. Franco-Villafañe et al., Phys. Rev. Lett., **111**, 170405 (2013).
6) L.P. Hughston, Proc. Roy. Soc. Lond. **A 383**, 459-466 (1982).
7) M. Moshinsky and A. Szczepaniak, J. Phys. A: Math Gen., **22** L817-L819 (1989).
8) R.P. Martínez. H.N. Núñez-Yépez and A.L. Salas-Brito, Eur. J. Phys., **15**, 135-141 (1995).
9) Z.F. Li et al., J. Math. Phys., **46**, 103514 (2005).
10) I. Bars, Phys. Rev. D, **79**, 045009 (2009).
11) R. Gerritsma et al., Nature, **463**, 78-71 (2010).
12) P.C. Clemnov and J.W. Willson, Proc. Roy. Soc. **A 237**, 117-131 (1956).
13) B. Buti, Phys. Fl., **6**, 89-99 (1963).
14) E.V. Chizhonkov, A.A. Frolov and L.M. Gorbunov, Russ. J. Numer. Anal. Math. Modelling, **23**, 455-467 (2008).
15) C.B. Schroeder, J. Phys.: Conf. Ser., **169**, 012007 (2009).
16) E.V. Chizhonkov and A.A. Frolov, Russ. J. Numer. Anal. Math. Modelling, **26**, 379-396 (2011).
17) C. Maity, N. Chakrabarti and S. Sengupta, J. Math. Phys., **52**,043101 (2011).
18) A. Marinelli, E. Hemsing and B. Rosenzweig, Phys. Plasmas, **19**, 063108 (2012).
19) E.V. Chizhonkov, Russ. J. Numer. Anal. Math. Modelling, **32**, 13-26 (2017).
20) A.A. Frolov and E.V. Chizhonkov, Comp. Math. & Math. Phys., **57**, 1808-1821 (2017).
21) E.V. Chizhonkov and A.A. Frolov, Russ. J. Numer. Anal. Math. Modelling, **34**, 71-84 (2019).
22) A.A. Frolov and E.V. Chizhonkov, Phys. Scr., **98**, 065604 (2020).
23) A.A. Frolov and E.V. Chizhonkov, Russ. J. Numer. Anal. Math. Modelling, **60**, 503-519 (2020).
24) O.S. Rozanova and E.V. Chizhonkov, Doklady Math., **101**, 254-256 (2020).
25) R. Penfield and H. Zatzkis, J. Franklin Inst., 121-125 (1956).
26) N.W. Taylor, J. Austral. Math. Soc., **2**, 206-208 (1961).
27) T.P. Mithchell and D.L. Pope, J. Soc. Indust. Appl. Math. **10**, 49-61 (1962).
28) E.H. Hutten, Nature, **205**, 892 (1965); Nature, **207**, 854 (1965).
29) W. Moreau, R. Easther, and R. Neutze, Am. J. Phys. **62** (6), 531–535 (1994).

30) R.E. Mickens, J. Sound & Vibrations, **212**, 905-908 (1998).
31) A. Beléndez and C. Pascual, Phys. Lett., **A 371**, 291-299 (2007).
32) A. Beléndez et al., Phys. Scr., **77**, 025004 (2008).
33) J. Biazar and M. Hosami, J. Egypt. Math. Soc., **22**, 45-49 (2014).
34) P. Chakraborty, Sch. J. Phys., **2**, 349-352 (2015).
35) E. Parker, Gen. Relativ. Gravit., **106**, 49 (2017).
36) C. Grossert, M. Leder and M. Weitz, J. Mod. Optics, **63**, 1805-1813 (2016).
37) K.M. Fujiwara et al., New J. Phys., **20**, 063027 (2018).
38) Poincaré, *Les Methods Nouvelles de la Mécanique Célest*, t. 1 (Gauthier-Villars, Paris, 1892) (Dover, new York, 1957).
39) S. Lie, *Theorie der Trasfomationgruppen* (Teubner, Leipzig, 1888).
40) G.D. Birkhoff, *Dynamical Systems (Am. Math. Soc.*, New York, 1927).
41) G.I. Hori, Publ. Astr. Soc. Japan **21**, 567-587 (1971).
42) V.I. Arnold, *Geometrical Methods in the Theory of Differential Equations* (Springer, New York, 1988).
43) A.D. Bruno, *Local Methods in Nonlinear Differential Equations* (Springer, Berlin, 1989).
44) J. Guckenheimer and P. Holmes, *Nonlinear Oscillations, Dynamical Systems and Bifurcations* (Springer, New York, 1983).
45) J. Murdock, *Normal Forms and Unfoldings for Local Dynamical Systems* (Springer, New York, 2003).
46) L. A. MacColl, Am. J. Phys., **25**, 535-539 (1957)/
47) I.S. Gradshteyn and I.M. Ryzhik, *Tables of Integrals, Series and Products*, 7th edition, Elsevier (2007).

Figure Captions

Fig. 1: Phase space plots of solution of Eq. (1) in terms of dimensionless entities (Eq. 9). From inner to outer plot: β =0.1, 0.5, 0.999.

Fig. 2 Phase-space plots, numerical solution of Eq. (11).

Fig. 3 $\eta(\theta)$ vs. θ, numerical solution of Eq. (11).

Fig. 4 η' (θ) vs. θ, numerical solution of Eq. (11). Horizontal lines are maximal values of η'.

Fig. 5 Error in approximate solution for $\eta(\theta)$ (Eq. 23) relative to numerical solution of Eq. (11), β = 0.8.

Fig. 6 Error in approximate velocity $\eta'(\theta)$ computed from Eq. (23) relative to numerical solution of Eq. (11), β = 0.8.

Fig. 7 Phase-space plots showing evolution of deviation of approximate solution (through $O(\beta^6)$, Eq. (23)) from numerical solution of Eq. (11) for high β. Continuous: numerical solution; Dashed: Approximate solution.

Fig. 8 Error in approximate solution for $\eta(\theta)$ (Eq. 23) relative to numerical solution of Eq. (11), β = 0.99.

Fig. 9 Error in approximate velocity $\eta'(\theta)$ computed from Eq. (23) relative to numerical solution of Eq. (11), β = 0.99.

Fig. 10 Comparison between the $O(\mu^2)$ approximation to the velocity, $\eta'(\theta)$ (using Eq. (33), dashed) and the numerical solution of Eq. (11). μ =0.1. Dotted line – constant limit of velocity beyond turning point.

Fig. 11 Comparison between $O(\mu^2)$ approximation to $\eta(\theta)$ (Eq. (33), dashed) and numerical solution of Eq. (11). μ =0.1;

Fig. 12 Comparison between the $O(\mu^2)$ approximation to the position, $\eta(\theta)$ (Eq. (33), dashed) and the numerical solution of Eq. (11) near the turning point. μ =0.1.

Fig. 13 Relative error between $O(\mu^2)$ approximation to velocity, $\eta'(\theta)$ (using Eq. (33)) and numerical solution of Eq. (11). μ =0.1.

Fig. 14 Fourier coefficients of $\eta'(\theta)$, from numerical solution of Eq. (11), and spectrum of Eq. (35).

Fig. 15 Fourier coefficients of $\eta'(\theta)$ for approximate solution, Eqs (28) and (32) and from numerical solution of Eq. (11). μ = 0.2.

Figures

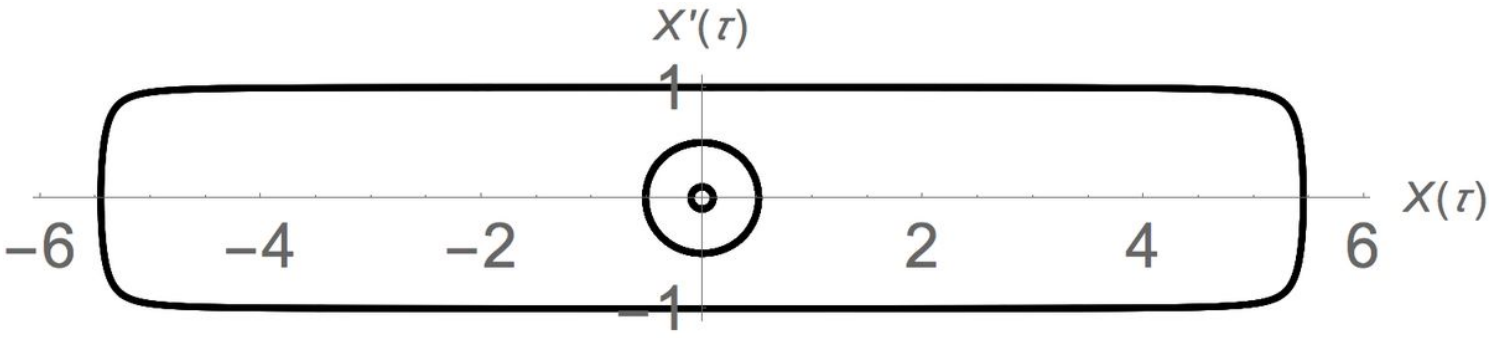

Figure 1

Phase space plots of solution of Eq. (1) in terms of dimensionless entities (Eq. 9). From inner to outer plot: b =0.1, 0.5, 0.999.

Figure 2

Phase-space plots, numerical solution of Eq. (11).

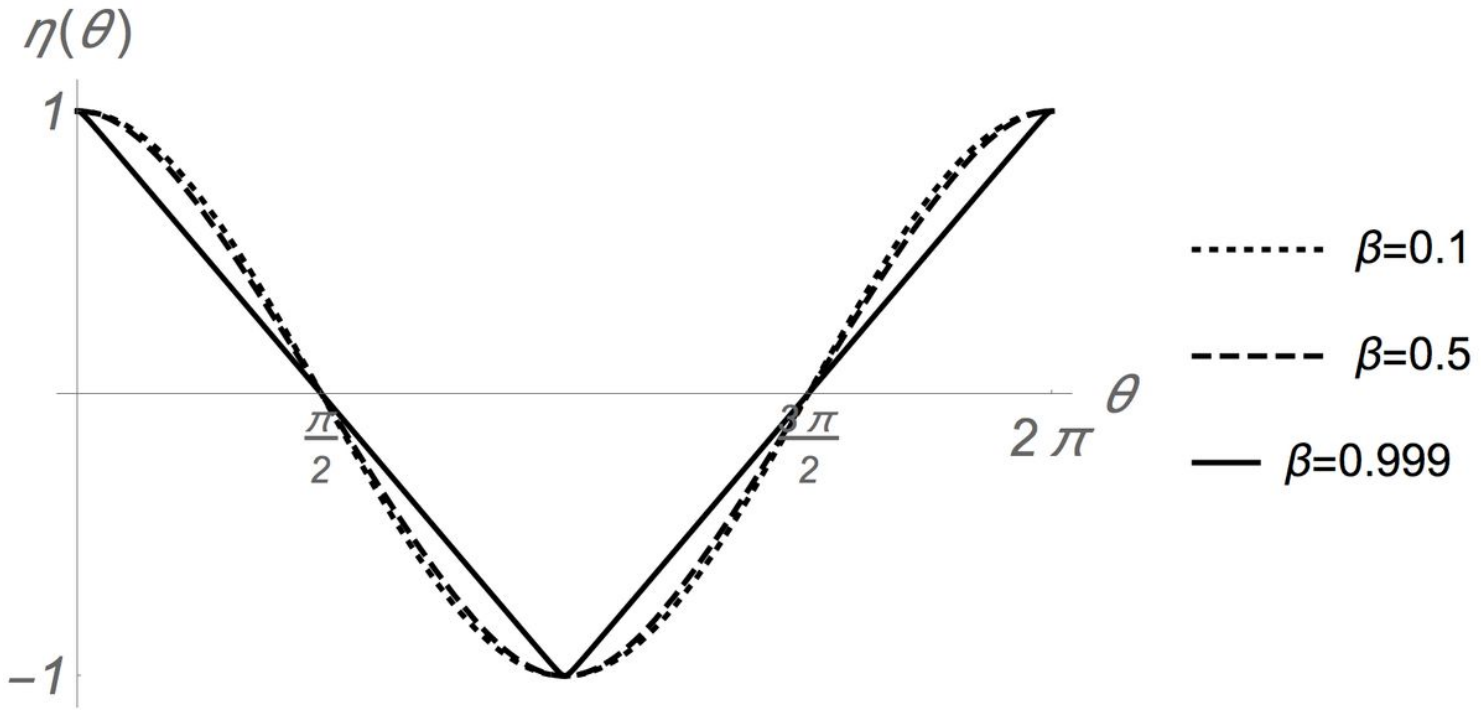

Figure 3

$h(q)$ vs. q, numerical solution of Eq. (11).

Figure 4

h□ (q) vs. q, numerical solution of Eq. (11). Horizontal lines are maximal values of h□.

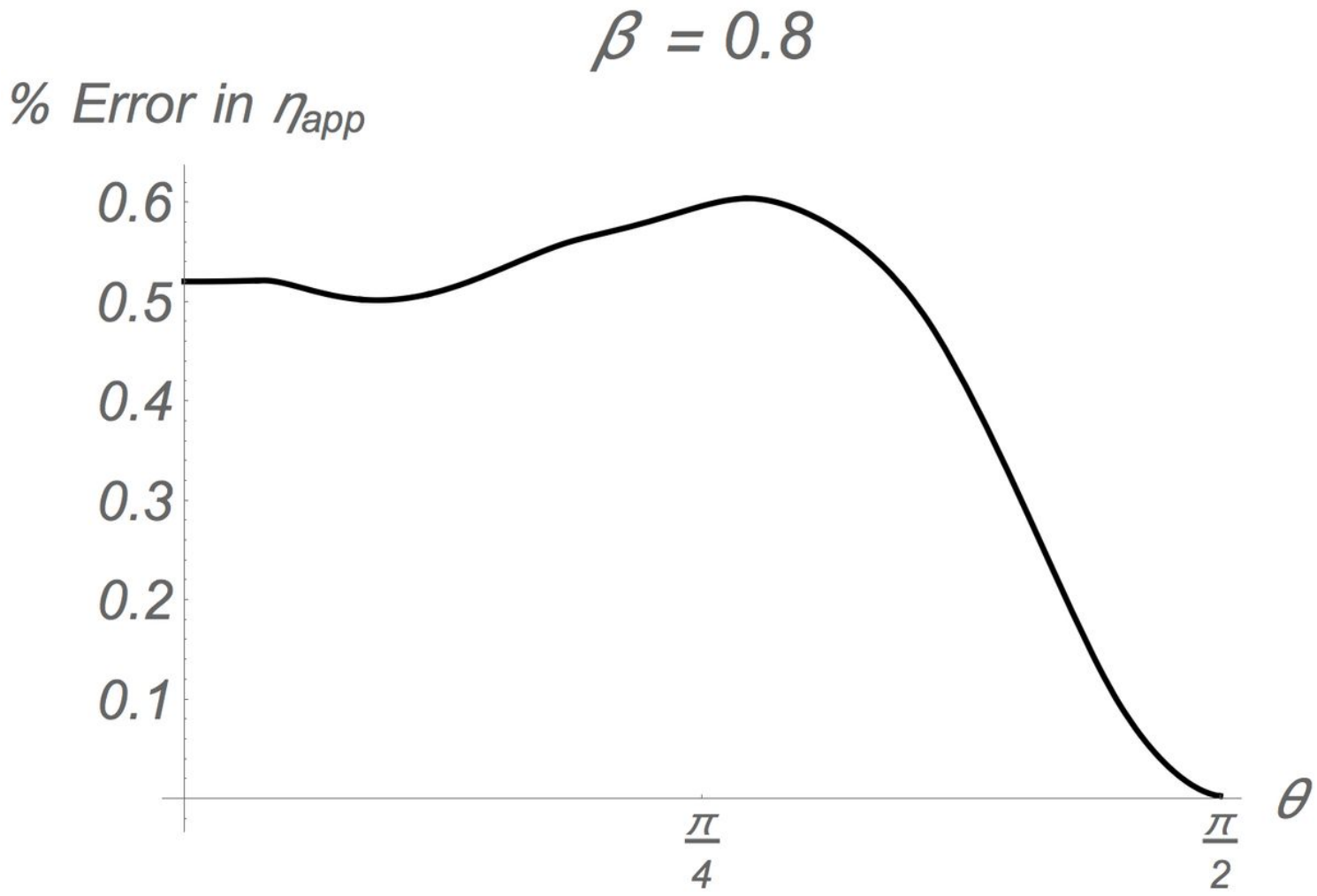

Figure 5

Error in approximate solution for $h(q)$ (Eq. 23) relative to numerical solution of Eq. (11), b = 0.8.

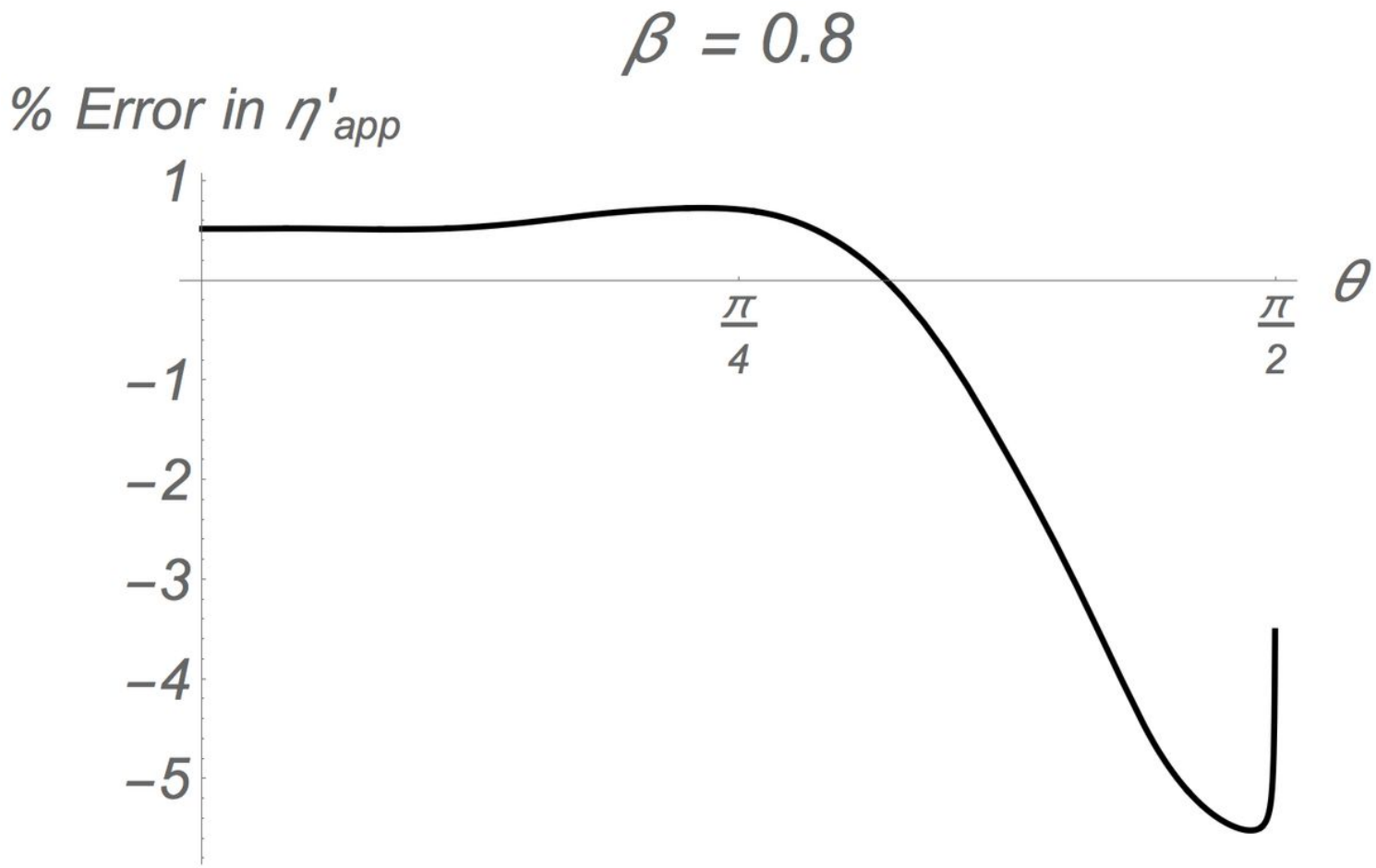

Figure 6

Error in approximate velocity $h'(q)$ computed from Eq. (23) relative to numerical solution of Eq. (11), b = 0.8.

Figure 7

Phase-space plots showing evolution of deviation of approximate solution (through $O(b^6)$, Eq. (23)) from numerical solution of Eq. (11) for high b. Continuous: numerical solution; Dashed: Approximate solution.

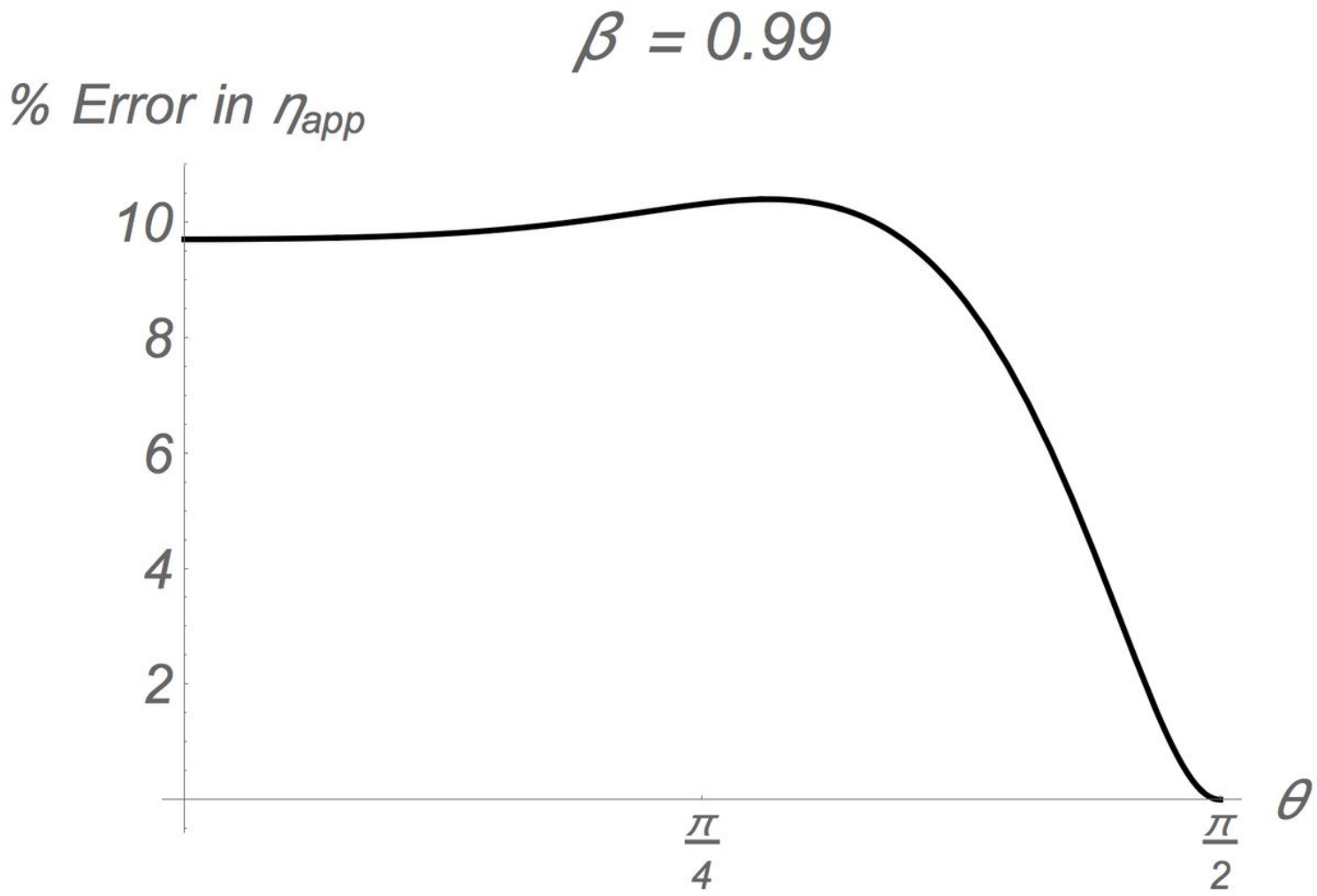

Figure 8

Error in approximate solution for $h(q)$ (Eq. 23) relative to numerical solution of Eq. (11), $b = 0.99$.

Figure 9

Error in approximate velocity $h'(q)$ computed from Eq. (23) relative to numerical solution of Eq. (11), $b = 0.99$.

Figure 10

Comparison between the $O(m^2)$ approximation to the velocity, $h'(q)$ (using Eq. (33), dashed) and the numerical solution of Eq. (11). m =0.1. Dotted line – constant limit of velocity beyond turning point.

Figure 11

Comparison between $O(m^2)$ approximation to $h(q)$ (Eq. (33), dashed) and numerical solution of Eq. (11). m =0.1;

Figure 12

Comparison between the $O(m^2)$ approximation to the position, $h(q)$ (Eq. (33), dashed) and the numerical solution of Eq. (11) near the turning point. m =0.1.

Figure 13

Relative error between $O(m^2)$ approximation to velocity, $h'(q)$ (using Eq. (33)) and numerical solution of Eq. (11). m =0.1.

Figure 14

Fourier coefficients of $h¢(q)$, from numerical solution of Eq. (11), and spectrum of Eq. (35).

Figure 15

Fourier coefficients of $h¢(q)$ for approximate solution, Eqs (28) and (32) and from numerical solution of Eq. (11). m = 0.2.